A climate sensitivity estimate using Bayesian fusion of instrumental observations and an Earth System model

R. Olson [*,1], R. Sriver [1], M. Goes[2,3], N. M. Urban[4], H. D. Matthews[5], M. Haran[6] and K. Keller[1,7]

[1] Department of Geosciences, Penn State University, University Park, PA, USA

[2] Cooperative Institute for Marine and Atmospheric Studies, University of Miami, Miami, FL, USA

[3] Atlantic Oceanographic and Meteorological Laboratory, NOAA, Miami, FL, USA

[4] Program in Science, Technology, and Environmental Policy (STEP), Woodrow Wilson School of Public and International Affairs, Princeton University, Princeton, NJ, USA

[5] Department of Geography, Planning and Environment, Concordia University, Montreal, QC, Canada

[6] Department of Statistics, Penn State University, University Park, PA, USA

[7] Earth and Environmental Systems Institute, Penn State University, University Park, PA, USA.

*Corresponding author email: rzt2-wrk@psu.edu

Abstract. Current climate model projections are uncertain. This uncertainty is partly driven by the uncertainty in key model parameters such as climate sensitivity (CS), vertical ocean diffusivity (K_v), and strength of anthropogenic sulfate aerosol forcing. These parameters are commonly estimated using ensembles of model runs constrained by observations. Here we obtain a probability density function (pdf) of these parameters using the University of Victoria Earth System Climate Model (UVic ESCM) - an intermediate complexity model with a dynamic three-dimensional ocean.

Specifically, we run an ensemble of UVic ESCM runs varying parameters that affect CS, ocean vertical diffusion, and the effects of anthropogenic sulfate aerosols. We use a statistical emulator that interpolates the UVic ESCM output to parameter settings where the model was not evaluated. We adopt a Bayesian approach to constrain the model output with instrumental surface temperature and ocean heat observations. Our approach accounts for the uncertainties in the properties of model-data residuals. We use a Markov chain Monte Carlo method to obtain a posterior pdf of these parameters.

The mode of the climate sensitivity estimate is 2.8 °C, with the corresponding 95% credible interval ranging from 1.8 to 4.9 °C. These results are generally consistent with previous studies. The CS pdf is sensitive to the assumptions about the priors, to the effects of anthropogenic sulfate aerosols, and to the background vertical ocean diffusivity. Our method can be used with more complex climate models.

1. Introduction

Climate hindcasts and projections are strongly affected by two key climate model parameters: climate sensitivity (CS) and vertical ocean diffusivity. Meridional overturning circulation, global temperature, and ocean heat accumulation that produces thermosteric sea level rise are good examples of climate variables that depend on these parameters [*Goes et al.*, 2010; *Knutti et al.*, 2002]. Better characterization of the uncertainty in these parameters is thus critical for future climate prediction.

Climate sensitivity is defined as the equilibrium near-surface temperature response to a doubling of atmospheric CO_2. CS is a measure of climate feedbacks that amplify or dampen the direct response of near-surface temperature to radiative forcings [*Andronova et al.*, 2007]. Vertical ocean diffusivity is a parameter that influences heat uptake by the ocean. It parametrizes mixing processes below the grid scale of climate models. For the same climate sensitivity, at higher diffusivities the atmosphere will reach the equilibrium temperature specified by CS more slowly, due to more heat flux into the deep ocean [NAS, 1979].

In order to estimate these parameters from climate models and observations, one needs to know past climate forcings. Both parameter estimation studies and simple theoretical considerations show that assumptions about these forcings influence climate sensitivity estimates and the uncertainty surrounding them [*Andreae et al.*, 2005; *Tanaka et al.*, 2009; *Urban and Keller*, 2010]. For example, *Andreae et al.* [2005] use a zero-dimensional climate model to illustrate that when they assume no aerosol effects, a climate sensitivity of just 1.3 °C is needed to explain the observed 1940-2000 warming. On the other hand, aerosol forcing of -1.7 W m^{-2} (a value that is within the IPCC range [*Forster et al.*, 2007]) requires a climate sensitivity of more than 10 °C [*Andreae et al.*, 2005]. Out of the main climate forcings, the forcings due to aerosols are especially uncertain. A large part of this uncertainty is due to anthropogenic sulfate aerosols [*Forster et al.*, 2007].

Parameters controlling climate sensitivity, vertical diffusion in the ocean, and strength of anthropogenic sulfate aerosols are commonly estimated using model runs and observations [*Knutti et al.*, 2002, 2003; *Forest et al.*, 2002, 2006; *Drignei et al.*, 2008; *Tomassini et al.*, 2007; *Edwards et al.*, 2007; *Sanso and Forest*, 2009]. Typically, an ensemble of model runs is used where the key parameters are systematically varied. The outputs from these runs are then compared with the observations, and the posterior probability distribution functions (pdfs) for model parameters are derived.

One conceptually simple methodology selects only the model runs that are consistent with the observations using a broad, heuristic approach [*Knutti et al.*, 2003]. In this framework all parameter combinations that pass the consistency criterion are assigned a uniform probability, while those that do not pass it receive a zero probability. These probabilities are then used to construct the posterior pdfs.

A more complex approach uses Bayesian statistics. This approach requires: (i) a model ensemble, (ii) observations, (iii) a statistical model that relates climate model output to the observations, and (iv) prior information about the model parameters (priors). In this framework, each parameter combination is associated with a likelihood that depends on how well the corresponding model output matches the observations [*Tomassini et al.*, 2007; *Sanso and Forest*, 2009]. The likelihood, $L(Y|\Theta)$, describes the degree of belief that the physical observations Y came from a climate model and a statistical model (describing the properties of data-model residuals) with unknown parameters Θ. Once the statistical model is defined, the likelihood $L(Y|\Theta)$ can be calculated from the residuals between the model output and the observations. In the Bayesian framework, the posterior probability of the unknown parameters given the observations is proportional to $L(Y|\Theta)$, and to the prior probability of the parameters:

$$p(\Theta|Y) \propto L(Y|\Theta) \times p(\Theta). \tag{1}$$

While the posterior probability $p(\Theta|Y)$ can be evaluated on a grid of parameter values, this can become too computationally expensive if the parameter space is multidimensional. In such cases Markov Chain Monte Carlo (MCMC) methods [*Metropolis et al.*, 1953; *Hastings*, 1970] can be used. The MCMC generates a sequence of parameter values (a Markov chain) which may be treated approximately as samples from the posterior distribution. Hence, virtually any property of the posterior distribution can be approximated by a corresponding sample property of this sequence.

Intermediate Complexity Earth System models are frequently used for this analysis [*Forest et al.*, 2002, 2006; *Knutti et al.*, 2003; *Tomassini et al.*, 2007; *Sanso and Forest*, 2009]. The appeal of these models is that they can be run at many parameter settings with relative ease. At the same time these models still represent many relevant physical processes. While the models can be run hundreds of times, many more runs at arbitrary parameter values are needed for the MCMC sampling. To approximate model output at these values, emulators (statistical approximators of climate models) can be used [e.g., *Drignei et al.* [2008]; *Holden et al.* [2010]; *Edwards et al.* [2010]]. The emulators draw on information about model outputs at known parameter settings to interpolate the output to any desired parameter setting.

In this study, we use the University of Victoria Earth System Climate Model (UVic ESCM) to estimate these important climate parameters. We constrain the ensemble of model runs with atmospheric surface temperature and ocean heat content observations to present probability distribution functions for key model parameters controlling the processes described above: climate sensitivity CS, background vertical ocean diffusivity K_{bg}, and a scaling parameter for the direct effects of anthropogenic sulfate aerosols A_{sc}. The use of the full 3D ocean allows for the representation of the non-linear effects of K_{bg} on ocean dynamics and currents (e.g., on the Meridional Overturning Circulation). We present posterior joint and marginal pdfs for the parameters, and explore the sensitivity of the results to prior assumptions.

2. Earth System Model, its Emulator, and Observational Constraints

2.1. Model Description

We use the University of Victoria Earth System Climate Model (UVic ESCM) [*Weaver et al.*, 2001] for our analysis. The atmospheric component is a one-layer energy-moisture balance model, with winds prescribed using the NCAR/NCEP climatology. The oceanic component is a three-dimensional model MOM2 [*Pacanowski*, 1995]. Both the atmospheric and the oceanic components have horizontal resolution of 1.8° (lat) × 3.6° (lon). The ocean has 19 depth levels. The model also includes terrestrial vegetation and carbon cycle [*Cox*, 2001], oceanic biogeochemistry based on *Schmittner et al.* [2005], and thermodynamic sea ice. We use the modified 2.8 version of the model. Specifically, we use a newer solar forcing, and include new transient forcings. The new forcings are described in Section 2.3.

2.2. Model parameters

2.2.1. Climate Sensitivity (*CS*)

Climate sensitivity is defined as the equilibrium response of global average near-surface temperature to a doubling of atmospheric CO_2. Climate sensitivity is a diagnosed parameter in the UVic ESCM. We vary CS through an additional parameter f^* that perturbs local outgoing longwave radiation:

$$Q^*_{PLW} = Q_{PLW} + f^*(T_t - T_0). \tag{2}$$

Here T_o is temperature at equilibrium (i.e. at the start of the transient run), T_t is a temperature at time t, Q_{PLW} is the planetary outgoing longwave radiation as calculated in the standard 2.8 version of the model and Q^*_{PLW} represents the modified outgoing longwave radiation. This approach is similar to *Matthews and Caldeira* [2007] and *Zickfeld et al.* [2009], but here the temperature terms are functions of latitude and longitude.

While f^* is the input parameter to the model, we want to know the CS values for each ensemble model run (Section 2.3). We determine the relationship between f^* and CS using a small number of CO_2 doubling experiments with varying f^* values at $K_{bg} = 0.1$ cm^2 s^{-1}. The runs continue for 2250 years to capture the equilibrium response of the model to CO_2. The CS is diagnosed as the average global temperature during the last 50 years of the runs minus the 50 year average prior to doubling. This mapping neglects a potential dependency of CS on K_{bg} at the same value of f^*. We adopt a prior range for CS from 1.1 to 11.2 (Table 1).

2.2.2. Background Vertical Ocean Diffusivity (K_{bg})

The rate at which surface temperatures adjust to radiative forcings is controlled by the rate at which heat is absorbed by the ocean. The vertical mixing of heat in the ocean is parameterized in UVic ESCM by a vertical diffusivity parameter K_v, which has contributions from tidal and background diffusivities [*Schmittner et al.*, 2009]:

$$K_v = K_{tidal} + K_{bg}. \tag{3}$$

K_{tidal} uses the parameterization of *St. Laurent et al.* [2002] following the methodology of *Simmons et al.* [2004]. The background diffusivity K_{bg} is assumed to be globally uniform. We vary K_{bg} to obtain different vertical ocean diffusivities (K_v), while keeping standard parameters for K_{tidal}. In our model, K_{bg} largely determines the total diffusivity in most areas of the pelagic pycnocline since the tidal component is small in those areas [*St. Laurent et al.*, 2002; *Schmittner et al.*, 2009]. As in *Schmittner et al.* [2009] and *Goes et al.* [2010], the model is modified to limit K_v to ≥ 1 cm^2 s^{-1} in the Southern Ocean below 500 m for better agreement with observations. Following *Goes et al.* [2010], we adopt the prior range for K_{bg} from 0.1 to 0.5 cm^2 s^{-1} (Table 1).

2.2.3. Anthropogenic Aerosol Scaling Factor (A_{sc})

Direct anthropogenic sulfate effects are modeled through spatially-resolved sulfate albedos Δa_s following *Matthews et al.* [2004] and *Charlson et al.* [1991] according to:

$$\Delta a_s = A_{scl} \frac{\beta \tau (1 - \alpha_s)^2}{cos(Z_{eff})}. \tag{4}$$

Here $\beta = 0.29$ is the upward scattering parameter, τ is the aerosol optical depth field, α_s is surface albedo, and Z_{eff} is the effective solar zenith angle. The strength of anthropogenic sulfate aerosol effects is modulated via the scaling parameter (A_{sc}). This parameterization does not account for the indirect effects of the sulfates on clouds. However, the indirect effects were found to be roughly proportional to the direct effects on major components of the Earth's radiation budget and climate on the global scale under idealized climate in a study by *Bauer et al.* [2008]. We use the prior range for A_{sc} from 0 to 3 (Table 1).

2.3. Hindcast Model Runs

We run an ensemble of UVic ESCM model runs where we systematically vary the three parameters over their prior ranges. Specifically, K_{bg} is varied on a uniform grid with values of (0.1, 0.2, 0.3, 0.4, 0.5) cm^2 s^{-1}. We sample CS at (1.14, 1.64, 2.15, 2.62, 3.11, 3.98, 5.36, 6.51, 8.20, 11.2) °C. The samples for A_{sc} are (0, 0.75, 1.5, 2.25, 3). These values form a quasi-cubic grid (Figure 4).

We spin the model up from observed data fields for 3,500 years with forcings set at year 1800 values. The transient runs continue from year 1800 to the present using historic radiative forcings. Volcanic aerosols, anthropogenic sulfate aerosols, changes in solar constant, and additional greenhouse gases such as CH_4, N_2O and CFCs, are implemented following *Goes et al.* [2010]. Specifically, the volcanic radiative forcing anomalies are from *Crowley* [2000a, b] for the period from 1800-1850, and from *GISS* [2007] and *Sato et al.*

[1993] for years 1850 to 2000. We update the solar forcing using the data of *Krivova et al.* [2007]. The atmospheric CO_2 concentration forcing is from *Etheridge et al.* [1998] and *Keeling et al.* [2004], complemented by the RCP8.5 scenario data after year 2002 [*Moss et al.*, 2010; *Riahi et al.*, 2007].

2.4. Observational Constraints

We use two observational constraints. The first is global average atmospheric surface / ocean surface temperatures (T) from the HadCRUT3 dataset of the Hadley Center [*Brohan et al.*, 2006]. These observations are defined as anomalies with respect to the 1850-1899 period average. The observations cover the time period from 1850 to 2006 (Figure 2). The second constraint is global total ocean heat content (OHC) in the 0-700 m layer [*Domingues et al.*, 2008]. These observations span the period from 1950 to 2003, and are calculated as anomalies with respect to the whole observation period (Figure 2). Modeled temperature and ocean heat content are converted to anomalies to be consistent with the observational constraints.

2.5. Gaussian Process Emulator

The MCMC sampling requires a large number of model runs (> 10000) at arbitrary parameter values. Since it is computationally infeasible to run UVic ESCM at that many parameter settings, we use a statistical emulator that can approximate the model outputs at any parameter value. We adopt Gaussian Process (GP) emulation. This technique was previously used to approximate climate models by *Bhat* [2010], *Sanso and Forest* [2009] and *Rougier et al.* [2009]. We emulate model output as a function of climate parameters separately for temperature and for ocean heat content. For each tracer, we develop separate emulators for each time step during the years for which the observations are available (Section 2.4). Thus, we build a total of 157 emulators for temperature, and 54 for the ocean heat content.

We define model output of tracer k at time t as $f_{t,k}(\theta)$ where θ is a vector of model parameters (K_{bg}, CS, A_{sc}). The $f_{t,k}(\theta)$ is only defined on a discrete set of parameter values where the model was run. The purpose of the emulator is to estimate a function $\tilde{f}_{t,k}(\theta)$ approximating model output on the continuous parameter ranges specified in Table 1. In the following discussion we will consider the emulator for atmospheric surface temperature at time t_0. The emulators for all other times and for the second tracer (ocean heat content) follow a similar statistical model. The indices t and k will thus be dropped from the rest of the emulator description.

The emulator is developed in linearly rescaled coordinates with transformed parameters $\theta'= (K'_{bg}, CS', A'_{sc})$ each taking on a range from zero to unity. The emulator approximates the climate model output as:

$$\tilde{f}(\theta') = P(\theta') + Z(\theta'), \tag{5}$$

where P is a quadratic polynomial in model parameters, and Z is a zero-mean Gaussian Process with an isotropic covariance function. Specifically, the covariance between Z at parameters θ'_i and θ'_j is modeled as $mC(i,j)$ where m is a scale multiplier and C is defined by:

$$C(i,j) = \exp \frac{-D_{ij}}{l}. \tag{6}$$

Here $D_{i,j}$ is the Euclidean distance between the two model parameter settings and l is a range parameter. Based on exploratory data analysis, we choose l=0.6. This formulation ensures that model output at nearby parameter settings is highly correlated (i.e. model output is a smooth function of the parameters). We choose a nugget variance σ_ϵ^2 of zero. This implies that the emulator is equal to model output at the points of the ensemble design grid.

We estimate the polynomial parameters and m. The polynomial parameters are the generalized linear squares estimates adjusting for the covariance function of the spatial process. They have a closed form solution that follows a standard formulation in Universal Kriging. m is likewise found by maximum likelihood given the parameter $\lambda = \sigma_\epsilon^2/m = 0$, and it has a closed form solution given λ as well (D. Nychka, personal communication). The optimized parameters provide the Best Linear Unbiased Estimate (BLUE) of $\tilde{f}(\theta')$ [*Furrer et al.*, 2010].

Emulators for other times and variables have different P and m. Henceforth all the emulators for all time steps and both tracers will be collectively referred to as the "emulator".

The emulator was extensively tested using the leave-one-out cross validation analysis. The emulator is found to perform adequately well (e.g., Figure 1) during the times when the variability of model output across the parameter space is high. The cross-validation errors are larger in the relative sense during the times close to the midpoints for the averaging periods for the anomalies (i.e. year 1870 for temperature, and 1980 for ocean heat content). At such times the signal is small and the model output is not a smooth function of the parameters, therefore it is impossible to accurately predict it based on the information from the remaining runs. We are unaware of any improvement in emulation techniques that could overcome this problem. We note that in this case the emulator errors are very low in the absolute sense and they are not expected to affect the estimation results. Overall, based on the cross-validation analysis, we are confident that the emulator provides a reasonable tool to interpolate model output.

3. Statistical Model and Markov Chain Monte Carlo

We use a Bayesian parameter estimation method. In order to be able to evaluate the likelihood of observations given the unknown parameters $L(Y|\Theta)$, we need a statistical model that defines the relationship between the model (and the emulator) output and the observations. We refer to the emulator output by $\tilde{f}_{t,k}(\theta)$ (for time t, tracer k, and parameter combination θ). The observations are denoted by $y_{t,k}$. We denote each observational time series by $\mathbf{y_k} = y_{1,k}, ..., y_{N_k,k}$ where N_k is the number of observations for tracer k. The set of all observations is referred to as $Y = (\mathbf{y_T}, \mathbf{y_{OHC}})$.

We assume that the discrepancy between the emulator and the observations is due to the time constant bias b_k and time-varying error $\epsilon_{t,k}$. Thus, our statistical model is:

$$y_{t,k} = \tilde{f}_{t,k} + b_k + \epsilon_{t,k}. \tag{7}$$

$\epsilon_{t,k}$ results from (i) model error, (ii) natural climate variability, (iii) emulator error, and (iv) observational error. We assume that $\epsilon_{t,k}$ is an autoregressive process of order 1 (AR1) with unknown AR1 parameters σ_k^2 and ρ_k. σ_k^2 represents the variance of the AR(1) innovations while ρ_k represents the autocorrelation of lag1 (i.e. correlation of $\epsilon_{t,k}$ with $\epsilon_{t-1,k}$). This form is chosen both for its simplicity and the ability to account for the uncertain autocorrelation in the error terms. The bias term b_k represents time-independent biases. Note that for ocean heat content we use anomalies with respect to the entire observational period. As a result, the average modeled and observed OHC is 0 by definition and we set b_{OHC} to 0. Our statistical model is similar to *Urban and Keller* [2010], although they do not incorporate bias terms.

For this statistical model, the likelihood of each observational time series $\mathbf{y_k}$ given the UVic ESCM model output and the statistical parameters $L(\mathbf{y_k}|\theta, \sigma_k, b_k, \rho_k)$ is given by [*Bence*, 1995] and is provided in the Appendix. We assume independence between the model-data residuals for different tracers. Under this assumption, the likelihood of both observations is equal to the product of the individual likelihoods: $L(Y) = L(\mathbf{y_1}) \times L(\mathbf{y_2})$. Denote the set of all parameters by $\Theta = (K_{bg}, CS, A_{sc}, \sigma_T, \rho_T, b_T, \sigma_{OHC}, \rho_{OHC})$. Using Bayes Theorem, the posterior probability of the parameters can be calculated as:

$$p(\Theta|Y) \propto L(Y|\Theta) \times p(\Theta) \qquad (8)$$

where $p(\Theta)$ is the prior for the parameters (Section 4).

Two distinct approaches to estimate the properties of the the error process ϵ are (i) from the observations or models [*Forest et al.*, 2006; *Tomassini et al.*, 2007], or (ii) directly from the model-data residuals together with the physical parameters [*Urban and Keller*, 2010; *Goes et al.*, 2010; *Tonkonojenkov*, 2010]. Here we use the second approach and estimate all parameters together in the MCMC step.

We draw samples from the joint posterior $p(\Theta|Y)$ using the MCMC algorithm [*Metropolis et al.*, 1953; *Hastings*, 1970] and generate the posterior probability distribution of Θ. Our MCMC prechains are 50,000 members long, while the final chain has 300,000 members. We use information from previous chain covariance to construct the proposal distribution for each subsequent chain following *Roberts and Rosenthal* [2009]. We test the chains for convergence using the MCMC standard errors from the consistent batch means procedure [*Flegal et al.*, 2008; *Jones et al.*, 2006], and by repeating the assimilation with different starting values of the parameters for the final chain. Neither of these checks suggest any issues with convergence. Hence, we are satisfied that our MCMC-based inference provides reasonable estimates of the posterior pdfs.

4. Priors

We run two assimilation experiments. In the base case experiment we use non-uniform priors for climate sensitivity and background vertical ocean diffusivity. We refer to this experiment as NON-UNIF. The priors for this experiment are listed in Table 1 and plotted in Figure 3. For K_{bg} the prior is Lognormal (-1.55, 0.59) cm^2 s^{-1} [*Bhat*, 2010]. This prior has a mode of 0.15 cm^2 s^{-1} and a mean of 0.24 cm^2 s^{-1}. The prior represents our prior belief that the values of 0.1 - 0.2 cm^2 s^{-1} are more likely than 0.4 - 0.5 cm^2 s^{-1} which is suggested by *Goes et al.* [2010] who use vertical oceanic tracer distributions to constrain K_{bg}. The climate sensitivity prior incorporates weak prior information derived from current mean climate and Last Glacial Maximum constraints. Specifically, we use a product of normal inverse Gaussian distributions (NIG) of $NIG(\alpha = 1.8, \delta = 2.3, \beta = 1.2, \mu = 1.7)$ and $NIG(\alpha = 1.9, \delta = 3.3, \beta = 1.0, \mu = 1.3)$. We choose these distributions for their empirical ability to simultaneously fit the lower, upper, and best estimates in *Knutti and Hegerl* [2008], not because we have any theoretical motivation for the NIG distribution. While the central tendencies of the two NIG pdfs are generally compatible with past studies, the distributions are not based on any specific pdf from any of these studies. The combined prior distribution for CS is shown in Figure 3. It has a mean of 3.25 °C, and the 90%

interval from 1.7 to 5.2 °C. We use uniform priors for A_{sc} and for all statistical parameters over the ranges specified in Table 1.

To explore the sensitivity of the results to priors, we run a second assimilation experiment, where all priors are uniform over the ranges shown in Table 1. We refer to this experiment as UNIF.

5. Results

5.1. Probabilistic Hindcasts

The probabilistic hindcasts capture the overall temporal structure of the observations (Figure 2). Specifically, the emulator is able to correctly represent the trend due to greenhouse warming (black line). We add an AR1 error process (representing model, observational, and emulator error, as well as the natural variability) to each emulator from the sub-sampled MCMC chain to produce the 95% credible intervals. In case of temperature, each emulator is corrected by adding a corresponding bias term from the chain. Overall, the method produces a reasonable surprise index (e.g., 1.9% of the ocean heat content and 5.1% of the temperature observations lie outside of the 95% hindcast range).

The surface air temperature from the best fit emulator illustrates the effects of the stratospheric volcanic aerosols, with several prominent short-term coolings associated with the eruptions. For some of these eruptions, such as Agung (1963) and Mount Pinatubo (1991), the modeled response matches the observations relatively well, while for others, such as Krakatoa (1883), the model displays considerable cooling that is not present in the observations. Some of this discrepancy might be due to the unresolved climate variability, and due to the uncertainty in the past volcanic radiative effects [*Ammann et al.*, 2003] and temperature observations.

5.2. Parameter Estimates

Under the baseline assumptions of non-uniform priors, posterior pdfs for climate sensitivity and vertical ocean diffusivity are broadly consistent with previous studies. The mode of the climate sensitivity pdf is 2.8 °C, and the mean is 3.1 °C. The 95% posterior credible interval ranges from 1.8 °C to 4.9 °C (Table 2). These values are broadly consistent with the likely range of 2 to 4.5 °C, and the most likely value of 3 °C given by the IPCC [*Solomon et al.*, 2007]. The mode is similar to results from *Forest et al.* [2006] and *Knutti et al.* [2003], and is slightly higher than in *Tomassini et al.* [2007].

For K_{bg}, we estimate a mode of 0.11 cm^2 s^{-1}, and a mean of 0.19 cm^2 s^{-1} (Table 2, Figure 3). The pdf for K_{bg} was reported to depend on the tracers used to constrain this parameter [*Schmittner et al.*, 2009]. The mode of the K_{bg} matches results of *Schmittner et al.* [2009] based on global vertical ocean profiles of CFC11, and of $\Delta^{14}C$, and is slightly lower than 0.15 cm^2 s^{-1} reported in [*Goes et al.*, 2010] based on profiles of three tracers. We stress that K_{bg} is not directly comparable with vertical diffusivities in other models [*Tomassini et al.*, 2007; *Kriegler*, 2005] because these parameters represent different processes. For example, our K_{bg} excludes tidally induced and Southern Ocean mixing, while the related K_v in *Kriegler* [2005] accounts for all vertical mixing processes. Therefore, our results should be interpreted as specific to our version of UVic ESCM.

The estimated aerosol scaling factor has the most likely value of 1.2. This is broadly consistent with the default assumptions on the aerosol effects in the UVic ESCM (which imply the value of 1). Estimation of A_{sc} should be interpreted with caution because A_{sc}

implicitly includes effects due to neglected forcings that might have emission or concentrations patterns similar to the anthropogenic sulfates. To better constrain A_{sc} it will be necessary to include these neglected forcings. Otherwise, one could interpret the value of A_{sc} as representing the combined effects of the aerosols as well as the neglected forcings. Similar to the case of K_{bg}, A_{sc} is a model specific parameter and can not be readily compared to results from other models [i.e. *Tanaka et al.* [2009]].

As in previous studies, the climate sensitivity pdf, and its upper tail in particular, are sensitive to the assumptions about the priors [e. g. *Forest et al.*, 2002, 2006; *Sanso and Forest*, 2009; *Tomassini et al.*, 2007; *Annan and Hargreaves*, 2011] (Figure 3). For example, replacing the expert prior with the uniform prior moves the upper bound of the 95% credible interval for CS to 10.2 °C (Table 2). This is in agreement with the results from *Forest et al.* [2006], but considerably higher than in *Annan and Hargreaves* [2011]. This discrepancy might be at least in part because *Annan and Hargreaves* [2011] consider a different type of constraint - Earth Radiation Budget Experiment (ERBE) data analyzed by *Forster and Gregory* [2006]. For the uniform prior, there is a considerable probability mass above the upper bound of the IPCC likely range of 4.5 °C (Figure 3), similar to previous studies (e.g., *Forest et al.* [2006]; *Knutti et al.* [2003]).

The use of uniform priors for climate sensitivity can be problematic as the posterior estimates are sensitive to the upper bound for the prior [*Annan and Hargreaves*, 2011]. In addition, such priors do not take independently collected evidence from other studies into account. High climate sensitivities become possible in this case because the flat prior assigns them high weight to begin with, while the constraint provided by the observations can be relatively weak. This suggests that it is crucial to use independent prior information during CS estimation whenever possible.

In addition, in the UNIF experiment the posterior pdf of K_{bg} is bimodal (Figure 3). Multimodal pdfs for K_{bg} have been previously reported by *Forest et al.* [2002] and *Tomassini et al.* [2007]. It is, thus far, unclear which physical mechanisms, if any, are driving this bimodality. Note that here we withhold information on vertical tracer distributions that is needed to constrain K_{bg} and that the bimodality essentially disappears once that constraint is introduced as a prior in the NON-UNIF case.

Joint bivariate pdfs for parameter pairs exhibit a complex structure (Figure 4), similar to the results from from *Tomassini et al.* [2007]. Although this is not visibly evident, there is some correlation between K_{bg} and CS. Specifically, the correlation is 0.24 in the NON-UNIF experiment, and 0.44 in the UNIF experiment. This is in agreement with 0.4 found in *Urban and Keller* [2010] even though the two studies differ in terms of climate models, observational constraints, and priors. It is difficult to compare these results with other studies ([e. g. *Tomassini et al.*, 2007; *Forest et al.*, 2002, 2006]) because they do not report the numerical value for the correlation coefficient while the pairs plots of the parameters can underestimate the correlation [*Urban and Keller*, 2010].

Climate sensitivity is even more strongly correlated with A_{sc}, meaning that for higher climate sensitivity, higher aerosol effects are needed to explain historical climate change. This agrees with results from *Andreae et al.* [2005] and *Tanaka et al.* [2009] and implies that reducing uncertainty in A_{sc} will help reduce uncertainty in climate sensitivity. Ruling out high values of A_{sc} is especially important, because this is where climate sensitivity pdf appears to be most sensitive to A_{sc} (Figure 4).

When the uniform priors on K_{bg} and CS are used, higher aerosol scaling values become possible, even though the prior on A_{sc} is the same in both cases. Because A_{sc} and CS are correlated, higher aerosol scalings are necessary to counteract higher warming due to larger climate sensitivities in the uniform prior case to match the observations.

Climate parameter estimation using a model with a 3D ocean (GENIE-1) has been previously performed by *Holden et al.* [2010] so it might be interesting to compare our methodology and results with that study. *Holden et al.* [2010] vary a much larger set of parameters and derive a pdf for climate sensitivity using a Last Glacial Maximum (LGM) tropical Sea Surface Temperature (SST) anomaly as a main constraint. They also indirectly use information from several global climate metrics through a pre-calibration procedure. In our study we consider an orthogonal set of constraints that includes information about the time-resolved response of climate to modern forcings. We also provide a probabilistic estimate of vertical ocean diffusivity K_{bg}. In terms of the ocean models used, *Holden et al.* [2010] employ a coarse resolution frictional geostrophic model. On the other hand, the resolution of UVic ESCM is much higher and the dynamics is based on the Navier-Stokes equations, subject to the hydrostatic and Boussinesq approximations. The statistical methodologies are different as well. In particular, our approach is fully Bayesian and we use explicit priors for all model parameters. Also, the statistical properties of the error process are assumed in *Holden et al.* [2010], while here we estimate them together with the physical model parameters. The mode of climate sensitivity found in *Holden et al.* [2010] is 3.6 °C under the favored set of assumptions, which is substantially higher than 2.8 °C in our baseline case of non-uniform priors. We cannot attribute this gap with certainty to any specific factor due to the number of differences between the studies.

6. Caveats

Our forthcoming conclusions are subject to several caveats. The first set of caveats deals with the Earth System model. Our model does not include all forcings (such as, sulfate effects on clouds or tropospheric ozone [*Forster et al.*, 2007]). The patterns of some of excluded forcings might be similar to anthropogenic sulfates, thereby biasing the A_{sc} estimates. Including thus far neglected forcings is the subject of future research. Also, we only consider a subset of uncertain climate parameters. Our results would change if these additional uncertainties were considered. The model relies on a number of simplifications. The representation of open ocean mixing is highly parametrized and ignores, for example, effects of transient upper ocean mixing processes, such as tropical cyclones, that have been shown capable of influencing upper-ocean temperature patterns through mixing of heat [*Sriver et al.*, 2010]. We vary the longwave radiation feedbacks to change climate sensitivity. In reality, the uncertainty in shortwave radiative feedbacks also contributes to the CS uncertainty [*Bony et al.*, 2006]. Also, we only use a single model and neglect the uncertainty in model response to external forcings [*Stouffer et al.*, 2006]. Finally, we do not fully account for past climate forcings uncertainties.

The second set of caveats is concerned with observations. When a short instrumental record is used, the results of our method can be influenced by natural climate variability and by observational errors comprising the residuals between the model and observations [*Tonkonojenkov*, 2010]. Adding more observations can improve the parameter estimates, as could using spatially resolved information.

Finally, limitations of the parameter estimation method deserve mentioning. We use a simplified likelihood function that does not account for the spectral complexity of the residuals, nor for the decrease of observational errors with time. Incorporating a more comprehensive likelihood function that captures a cross-correlation between the residuals for different tracers is the subject of future research.

7. Conclusions

Using a Bayesian approach, we fuse the UVic ESCM model with global observations to estimate background vertical ocean diffusivity (K_{bg}), climate sensitivity (CS), and the scaling parameter for the effects of anthropogenic sulfate aerosols (A_{sc}). Our methodology incorporates the effects of K_{bg} on 3D ocean dynamics. We use a Gaussian Process emulator to provide a fast surrogate for the climate model at arbitrary parameter combinations. The parameter estimates can be used to make climate projections using the UVic ESCM in future studies.

The mode for K_{bg} is similar to previous results obtained using oceanic tracers such as CFC11, temperature, and $\Delta^{14}C$ as constraints. The K_{bg} pdf is sensitive to the assumptions about the priors. If a uniform prior is used, then the results appear to show a bimodality, which is a potentially important result that might need further investigation.

Under the default assumptions of informative priors, the mode of climate sensitivity is 2.8 °C, with the 95% credible interval from 1.8 °C to 4.9 °C. This mode is consistent with many previous studies but lower than reported in *Holden et al.* [2010] who also use a 3D ocean model. As in previous studies, the upper tail of the CS pdf is sensitive to priors. The CS pdf depends critically on A_{sc}, with much higher climate sensitivities likely at high values of A_{sc}. The agreement with previous studies that use simpler climate models gives more confidence to using these models to estimate climate sensitivity.

Appendix

When the statistical model is defined as in Section 3, the likelihood of observational time series $\mathbf{y_k}$ coming from the model is given by [*Bence*, 1995]:

$$L(\mathbf{y_k}|\theta, \sigma_k, b_k, \rho_k) = \left(2\pi\sigma_{p,k}^2\right)^{-1/2} \exp\left(-\frac{1}{2}\frac{\epsilon_{1,k}^2}{\sigma_{p,k}^2}\right) \times$$
$$\times \left(2\pi\sigma_k^2\right)^{-(N_k-1)/2} \times \exp\left(-\frac{1}{2\sigma_k^2}\sum_{j=2}^{N_k} w_{j,k}^2\right).$$

Here $\sigma_{p,k}^2 = \sigma_k^2/(1-\rho_k^2)$ is stationary process variance, N_k is the number of observational data points for tracer k, and $w_{t,k} = \epsilon_{t,k} - \rho_k\epsilon_{t-1,k}, t > 1$ are whitened errors.

Acknowledgments. We thank Michael Eby and other UVic ESCM model developers for providing the model and for helpful discussions. Very productive and though-provoking discussions with David Pollard, Sham Bhat, Andreas Schmittner, and Chris Forest are gratefully acknowledged. This work would not have been possible without the contributions from scientists who compiled the datasets utilized in this study, and who helped to build and refine the UVic ESCM model. We thank two anonymous reviewers and K. Tanaka for very insightful and helpful reviews of the manuscript. This work was partially supported by NSF and USGS, as well as by the Canadian Foundation for Climate and Atmospheric Sciences (CFCAS GR-7059). All errors, views, and opinions are solely those of the authors.

References

Ammann, C. M., G. A. Meehl, W. M. Washington, and C. S. Zender (2003), A monthly and latitudinally varying volcanic forcing dataset in simulations of 20th century climate, *Geophys. Res. Lett.*, *30*(12), doi:10.1029/2003GL016875.

Andreae, M. O., C. D. Jones, and P. M. Cox (2005), Strong present-day aerosol cooling implies a hot future, *Nature*, *435*(7046), 1187–1190, doi:10.1038/nature03671.

Andronova, N., M. Schlesinger, S. Dessai, M. Hulme, and B. Li (2007), The concept of climate sensitivity: history and development, in *Human-induced Climate Change: An Interdisciplinary Assessment*, edited by M. Schlesinger, H. Kheshgi, J. Smith, F. de la Chesnaye, J. M. Reilly, T. Wilson, and C. Kolstad, Cambridge University Press.

Annan, J. D., and J. C. Hargreaves (2011), On the generation and interpretation of probabilistic estimates of climate sensitivity, *Clim. Change*, *104*(3-4), 423–436, doi:10.1007/s10584-009-9715-y.

Bauer, E., V. Petoukhov, A. Ganopolski, and A. V. Eliseev (2008), Climatic response to anthropogenic sulphate aerosols versus well-mixed greenhouse gases from 1850 to 2000 AD in CLIMBER-2, *Tellus Ser. B - Chem. Phys. Met.*, *60*(1), 82–97.

Bence, J. R. (1995), Analysis of short time series – Correcting for autocorrelation, *Ecology*, *76*(2), 628–639.

Bhat, K. G. (2010), Inference for complex computer models and large multivariate spatial data with applications to climate science, Ph.D. thesis, The Pennsylvania State University.

Bony, S., et al. (2006), How well do we understand and evaluate climate change feedback processes?, *Journal of Climate*, *19*(15), 3445–3482.

Brohan, P., J. J. Kennedy, I. Harris, S. F. B. Tett, and P. D. Jones (2006), Uncertainty estimates in regional and global observed temperature changes: A new data set from 1850, *J. Geophys. Res. [Atmos.]*, *111*(D12), doi:10.1029/2005JD006548.

Charlson, R. J., J. Langner, H. Rodhe, C. B. Leovy, and S. G. Warren (1991), Perturbation of the Northern-Hemisphere radiative balance by backscattering from anthropogenic sulfate aerosols, *Tellus Ser. A-Dyn. Met. Ocean.*, *43*(4), 152–163.

Cox, P. (2001), Description of the "TRIFFID" Dynamic Global Vegetation Model, *Tech. rep.*, Hadley Center technical note 24, Hadley Centre, Met Office, Berks, UK.

Crowley, T. J. (2000a), Causes of climate change over the past 1000 years, *Science*, *289*(5477), 270–277.

Crowley, T. J. (2000b), Causes of Climate Change Over the Past 1000 Years, IGBP PAGES/World Data Center for Paleoclimatology Data Contribution Series # 2000-045, NOAA/NGDC Paleoclimatology Program, Boulder CO, USA.

Domingues, C. M., J. A. Church, N. J. White, P. J. Gleckler, S. E. Wijffels, P. M. Barker, and J. R. Dunn (2008), Improved estimates of upper-ocean warming and multi-decadal sea-level rise, *Nature*, *453*(7198), 1090–U6, doi:10.1038/nature07080.

Drignei, D., C. E. Forest, and D. Nychka (2008), Parameter estimation for computationally intensive nonlinear regression with an application to climate modeling, *Ann. Appl. Stat.*, *2*(4), 1217–1230, doi:10.1214/08-AOAS210.

Edwards, N. R., D. Cameron, and J. Rougier (2010), Precalibrating an intermediate complexity climate model, *Clim. Dyn.*, Online First^{TM}, Retrived from http://www.springerlink.com/.

Edwards, T. L., M. Crucifix, and S. P. Harrison (2007), Using the past to constrain the future: how the palaeorecord can improve estimates of global warming, *Prog. Phys. Geog.*, *31*(5), 481–500, doi:10.1177/0309133307083295.

Etheridge, D. M., L. P. Steele, R. L. Langenfelds, R. J. Francey, J.-M. Barnola, and V. I. Morgan (1998), Historical CO_2 records from the Law Dome DE08, DE08-2, and DSS ice cores, in *Trends: A Compendium of Data on Global Change*, Carbon Dioxide Information Analysis Center, Oak Ridge National Laboratory, U.S. Department of Energy, Oak Ridge, Tenn., U.S.A.

Flegal, J. M., M. Haran, and G. L. Jones (2008), Markov Chain Monte Carlo: Can we trust the third significant figure?, *Statistical Science*, *23*(2), 250–260.

Forest, C. E., P. H. Stone, A. P. Sokolov, M. R. Allen, and M. D. Webster (2002), Quantifying uncertainties in climate system properties with the use of recent climate observations, *Science*, *295*(5552), 113–117.

Forest, C. E., P. H. Stone, and A. P. Sokolov (2006), Estimated PDFs of climate system properties including natural and anthropogenic forcings, *Geophys. Res. Lett.*, *33*(1), doi:10.1029/2005GL023977.

Forster, P., and J. Gregory (2006), The climate sensitivity and its components diagnosed from Earth Radiation Budget data, *J. Clim.*, *19*(1), 39–52, doi:10.1175/JCLI3611.1.

Forster, P., et al. (2007), Chapter 2: Changes in Atmospheric Constituents and in Radiative Forcing, in *Climate Change 2007: The Physical Science Basis. Contribution of Working Group I to the Fourth Assessment Report of the Intergovernmental Panel on Climate Change*, edited by S. Solomon, D. Qin, M. Manning, Z. Chen, M. Marquis, K. B. Averyt, M. Tignor, and H. L. Miller, Cambridge Univ. Press, Cambridge, United

Kingdom and New York, NY, USA.

Furrer, R., D. Nychka, and S. Sain (2010), *Package 'fields' manual*, retrieved from http://www.image.ucar.edu/Software/Fields/.

GISS (2007), Forcings in GISS climate model: stratospheric aerosol optical thickness, retrived from http://data.giss.nasa.gov/modelforce/strataer/tau_line.txt.

Goes, M., N. M. Urban, R. Tonkonojenkov, M. Haran, A. Schmittner, and K. Keller (2010), What is the skill of ocean tracers in reducing uncertainties about ocean diapycnal mixing and projections of the Atlantic Meridional Overturning Circulation?, *J. Geophys. Res.*, *115*, doi:10.1029/2010JC006407, C12006.

Hastings, W. K. (1970), Monte Carlo sampling methods using Markov chains and their applications, *Biometrika*, *57*(1), 97–109.

Holden, P. B., N. R. Edwards, K. I. C. Oliver, T. M. Lenton, and R. D. Wilkinson (2010), A probabilistic calibration of climate sensitivity and terrestrial carbon change in GENIE-1, *Clim. Dyn.*, *35*(5), 785–806.

Jones, G. L., M. Haran, B. S. Caffo, and R. Neath (2006), Fixed-width output analysis for Markov chain Monte Carlo, *Journal of the American Statistical Association*, *101*(476), 1537–1547, doi:10.1198/016214506000000492.

Keeling, C. D., T. P. Whorf, and the Carbon Dioxide Research Group (2004), Atmospheric CO_2 concentrations (ppmv) derived from in situ air samples collected at Mauna Loa Observatory, Hawaii, Scripps Institution of Oceanography (SIO), University of California, La Jolla, California, USA. Retrieved from http://cdiac.esd.ornl.gov/ftp/maunaloa-co2/maunaloa.co2.

Knutti, R., and G. C. Hegerl (2008), The equilibrium sensitivity of the Earth's temperature to radiation changes, *Nature Geosc.*, *1*(11), 735–743, doi:10.1038/ngeo337.

Knutti, R., T. F. Stocker, F. Joos, and G. K. Plattner (2002), Constraints on radiative forcing and future climate change from observations and climate model ensembles, *Nature*, *416*(6882), 719–723.

Knutti, R., T. F. Stocker, F. Joos, and G. K. Plattner (2003), Probabilistic climate change projections using neural networks, *Clim. Dyn.*, *21*(3-4), 257–272, doi:10.1007/s00382-003-0345-1.

Kriegler, E. (2005), Imprecise probability analysis for integrated assessment of climate change, Ph.D. thesis, University of Potsdam, Retrieved from http://opus.kobv.de/ubp/volltexte/2005/561/.

Krivova, N. A., L. Balmaceda, and S. K. Solanki (2007), Reconstruction of solar total irradiance since 1700 from the surface magnetic flux, *Astron. Astrophys.*, *467*(1), 335–346, doi:10.1051/0004-6361:20066725.

Matthews, H. D., and K. Caldeira (2007), Transient climate-carbon simulations of planetary geoengineering, *Proc. Natl. Acad. Sci. U. S. A.*, *104*(24), 9949–9954, doi: 10.1073/pnas.0700419104.

Matthews, H. D., A. J. Weaver, K. J. Meissner, N. P. Gillett, and M. Eby (2004), Natural and anthropogenic climate change: incorporating historical land cover change, vegetation dynamics and the global carbon cycle, *Clim. Dyn.*, *22*(5), 461–479, doi: 10.1007/s00382-004-0392-2.

Metropolis, N., A. W. Rosenbluth, M. N. Rosenbluth, A. H. Teller, and E. Teller (1953), Equation of state calculations by fast computing machines, *J. Chem. Phys.*, *21*(6), 1087–1092.

Moss, R. H., et al. (2010), The next generation of scenarios for climate change research and assessment, *Nature*, *463*(7282), 747–756, doi:10.1038/nature08823.

NAS (1979), Carbon dioxide and climate: A scientific assessment, *Tech. rep.*, US National Academy of Sciences, Washington, DC.

Pacanowski, R. C. (1995), MOM 2 documentation: Users' guide and reference manual, version 1.0., *Tech. Rep. 3*, GFDL Ocean Group, Geophysical Fluid Dynamics Laboratory, Princeton, New Jersey.

Riahi, K., A. Gruebler, and N. Nakicenovic (2007), Scenarios of long-term socio-economic and environmental development under climate stabilization, *Technological Forecasting and Social Change*, *74*(7), 887–935, doi:10.1016/j.techfore.2006.05.026.

Roberts, G. O., and J. S. Rosenthal (2009), Examples of Adaptive MCMC, *J. Comp. Graph. Stat.*, *18*(2), 349–367, doi:10.1198/jcgs.2009.06134.

Rougier, J., D. M. H. Sexton, J. M. Murphy, and D. Stainforth (2009), Analyzing the climate sensitivity of the HadSM3 Climate Model using ensembles from different but related experiments, *J. Clim*, *22*(13), 3540–3557, doi:10.1175/2008JCLI2533.1.

Sanso, B., and C. Forest (2009), Statistical calibration of climate system properties, *J. Royal Stat. Soc. Ser. C - App. Stat.*, *58*(Part 4), 485–503.

Sato, M., J. E. Hansen, M. P. McCormick, and J. B. Pollack (1993), Stratospheric aerosol optical depth, 1850-1990, *J. Geophys. Res.*, *98*, 22,987–22,994.

Schmittner, A., A. Oschlies, X. Giraud, M. Eby, and H. L. Simmons (2005), A global model of the marine ecosystem for long-term simulations: Sensitivity to ocean mixing, buoyancy forcing, particle sinking, and dissolved organic matter cycling, GB3004, *Global*

Biogeochem. Cycles, *19*(3), doi:10.1029/2004GB002283.

Schmittner, A., N. M. Urban, K. Keller, and H. D. Matthews (2009), Using tracer observations to reduce the uncertainty of ocean diapycnal mixing and climate-carbon cycle projections, GB4009, *Global Biogeochem. Cycles*, *23*, doi:10.1029/2008GB003421.

Simmons, H., S. Jayne, L. St. Laurent, and A. Weaver (2004), Tidally driven mixing in a numerical model of the ocean general circulation, *Ocean Mod.*, *6*(3-4), 245–263, doi:10.1016/S1463-5003(03)00011-8.

Solomon, S., et al. (2007), Technical summary, in *Climate Change 2007: The Physical Science Basis. Contribution of Working Group I to the Fourth Assessment Report of the Intergovernmental Panel on Climate Change*, edited by S. Solomon, D. Qin, M. Manning, Z. Chen, M. Marquis, K. B. Averyt, M. Tignor, and H. L. Miller, Cambridge University Press, Cambridge, United Kingdom and New York, NY, USA.

Sriver, R. L., M. Goes, M. E. Mann, and K. Keller (2010), Climate response to tropical cyclone-induced ocean mixing in an Earth system model of intermediate complexity, C10042, *Journal of Geophysical Research - Oceans*, *115*, doi:10.1029/2010JC006106.

St. Laurent, L., H. Simmons, and S. Jayne (2002), Estimating tidally driven mixing in the deep ocean, 2106, *Geophys. Res. Lett.*, *29*(23), doi:10.1029/2002GL015633.

Stouffer, R., et al. (2006), Investigating the causes of the response of the thermohaline circulation to past and future climate changes, *J. Clim.*, *19*(8), 1365–1387.

Tanaka, K., T. Raddatz, B. C. O'Neill, and C. H. Reick (2009), Insufficient forcing uncertainty underestimates the risk of high climate sensitivity, *Geophys. Res. Lett.*, *36*, doi:10.1029/2009GL039642, L16709.

Tomassini, L., P. Reichert, R. Knutti, T. F. Stocker, and M. E. Borsuk (2007), Robust Bayesian uncertainty analysis of climate system properties using Markov chain Monte Carlo methods, *J. Clim.*, *20*(7), 1239–1254, doi:10.1175/JCLI4064.1.

Tonkonojenkov, R. (2010), What is the skill of climate parameter estimation methods? A case study with global observational constraints, Master's thesis, The Pennsylvania State University, Retrieved from http://etda.libraries.psu.edu/theses/approved/WorldWideIndex/ETD-5159/index.html.

Urban, N. M., and K. Keller (2010), Probabilistic hindcasts and projections of the coupled climate, carbon cycle and Atlantic meridional overturning circulation system: a Bayesian fusion of century-scale observations with a simple model, *Tellus Ser. A - Dyn. Met. Ocean.*, *62*(5), 737–750, doi:10.1111/j.1600-0870.2010.00471.x.

Weaver, A. J., et al. (2001), The UVic Earth System Climate Model: Model description, climatology, and applications to past, present and future climates, *Atmos.-Ocean*, *39*(4), 361–428.

Zickfeld, K., M. Eby, H. D. Matthews, and A. J. Weaver (2009), Setting cumulative emissions targets to reduce the risk of dangerous climate change, *Proceedings of the National Academy of Sciences of the United States of America*, *106*(38), 16,129–16,134.

Figure Captions

Figure 1. Top row: scatterplot of the temperature anomaly (with respect to the 1850-2006 mean, [K]) emulator predictions vs. actual model output values for years 1870, 1940, and 2000. Specifically, each of the parameter combinations of the ensemble was taken out one at a time, and the emulator was trained on the remaining 249 ensemble members. Then the emulator was used to predict the missing value. The 1:1 line is also shown. Note that Y axis limits are different for each subplot. Bottom row: same for the ocean heat content anomalies (with respect to the 1950-2003 mean, $[1 \times 10^{22} J]$), for years 1960, 1980, and 2000. The emulator performance, of course, will be different for other times not shown here.

Figure 2. Probabilistic model hindcasts (grey shaded area), maximum posterior probability model output ('best fit', black line), and corresponding observations (red crosses) for the NON-UNIF assimilation experiment: (a) global average atmospheric surface temperature anomaly with respect to 1850-1899 mean [K] with corresponding observations of above surface / ocean surface temperatures from the HadCRUT3 dataset [*Brohan et al.*, 2006]; (b) upper ocean (0-700m) heat content anomaly with respect to 1950-2003 mean [1E22J], and observations from *Domingues et al.* [2008]. The grey area denotes the 95% credible intervals for model output taken from a 1000-member subsampled MCMC chain, with corresponding AR1 error processes (and bias terms for temperature) added. For the AR1 process simulations, the σ and ρ parameters were taken from the corresponding chain member. For the best fit model output for temperature, the maximum posterior probability model output was combined with the corresponding bias term.

Figure 3. Posterior pdfs (top row) and cdfs (bottom row) for model parameters obtained using both temperature and ocean heat content observations. Red: for the NON-UNIF experiment; blue: for the UNIF experiment. The dashed probability distribution lines represent the priors

used in the NON-UNIF experiment. The dashed whiskers in the box-and-whisker plots extend to the most extreme data point which is no more than 1.5 interquartile ranges from the box.

Figure 4. Bivariate joint pdfs for model parameters. Left: for the NON-UNIF experiment, right: for the UNIF experiment. The contour lines delineate the 90% and 95% posterior credible intervals. A 1000-member thinned MCMC chain is plotted using red dots. Parameters used for the UVic ESCM ensemble are shown in thick black circles.

Table 1: Prior ranges for the parameters used in the NON-UNIF experiment. Subscript T refers to the temperature data, and OHC refers to the ocean heat content data.

Parameter	Units	Lower Bound	Upper Bound	Prior Form
K_{bg}	cm^2 s^{-1}	0.1	0.5	Lognormal(-1.55, 0.59)
CS	°C per CO_2 doubling	1.1	11.2	$NIG(\alpha = 1.8, \delta = 2.3, \beta = 1.2, \mu = 1.7) \times NIG(\alpha = 1.9, \delta = 3.3, \beta = 1.0, \mu = 1.3)$
A_{sc}	unitless	0	3	uniform
σ_T	°C	0.01	inf	uniform
σ_{OHC}	1×10^{22} J	0.01	inf	uniform
ρ_T	unitless	0.01	0.99	uniform
ρ_{OHC}	unitless	0.01	0.99	uniform
b_T	°C	-0.51	0.50	uniform

Table 2: Properties of the posterior pdfs of all estimated parameters.

Parameter	Experiment	Mode	Mean	95% credible interval
K_{bg}	NON-UNIF	0.11	0.19	[0.10, 0.45]
	UNIF	0.11	0.30	[0.10, 0.50]
CS	NON-UNIF	2.8	3.1	[1.8, 4.9]
	UNIF	3.0	4.8	[1.6, 10.2]
A_{sc}	NON-UNIF	1.2	1.1	[0.35, 1.5]
	UNIF	1.6	1.2	[0.25, 1.8]
σ_T	NON-UNIF	0.10	0.10	[0.091, 0.11]
	UNIF	0.10	0.10	[0.091, 0.11]
σ_{OHC}	NON-UNIF	2.6	2.7	[2.2, 3.3]
	UNIF	2.6	2.7	[2.2, 3.3]
ρ_T	NON-UNIF	0.58	0.58	[0.44, 0.72]
	UNIF	0.58	0.58	[0.44, 0.72]
ρ_{OHC}	NON-UNIF	0.079	0.17	[0.018, 0.43]
	UNIF	0.091	0.17	[0.018, 0.42]
b_T	NON-UNIF	-0.031	-0.031	[-0.079, 0.021]
	UNIF	-0.034	-0.033	[-0.083, 0.022]

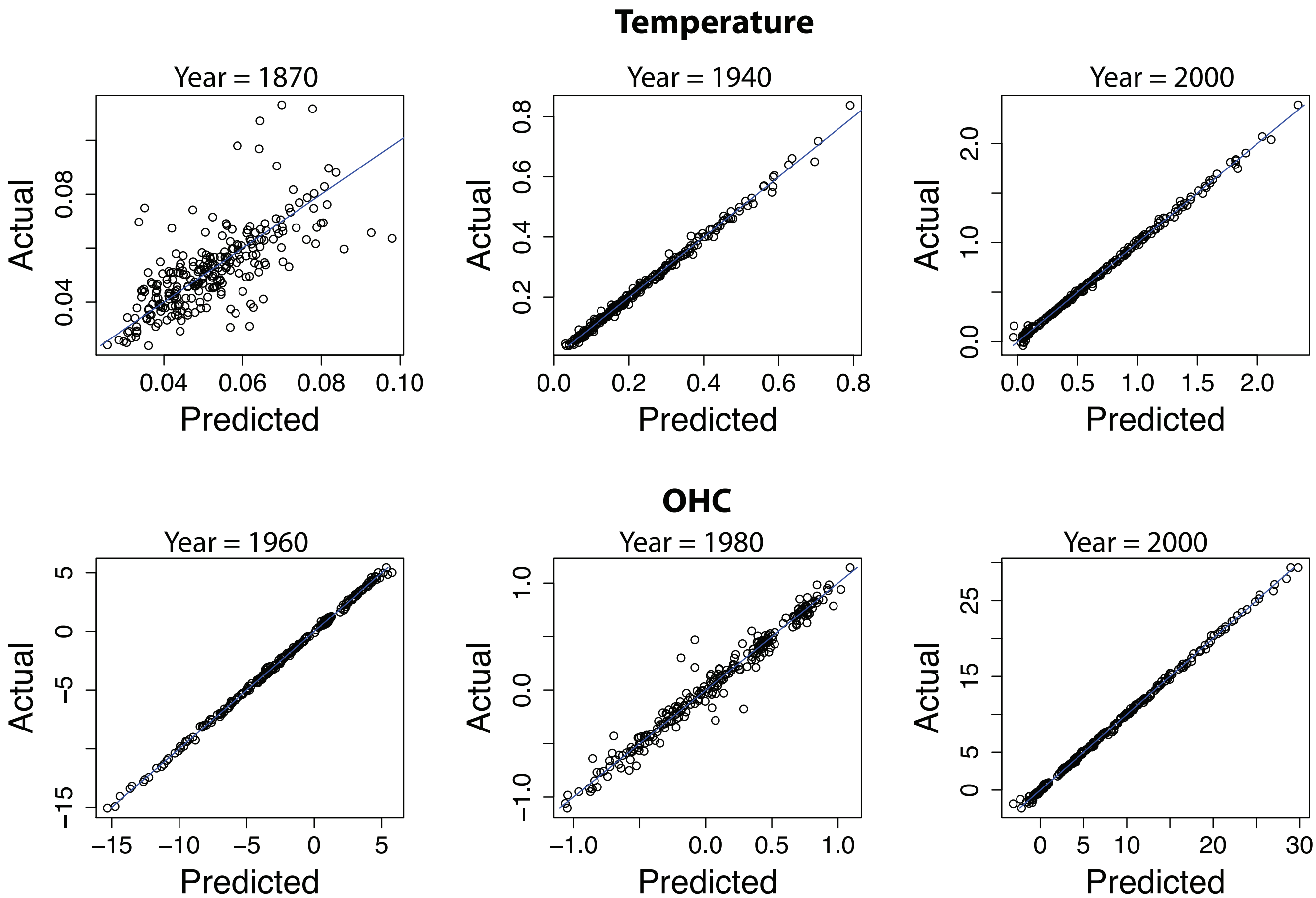

Figure 1: Top row: scatterplot of the temperature anomaly (with respect to the 1850-2006 mean, [K]) emulator predictions vs. actual model output values for years 1870, 1940, and 2000. Specifically, each of the parameter combinations of the ensemble was taken out one at a time, and the emulator was trained on the remaining 249 ensemble members. Then the emulator was used to predict the missing value. The 1:1 line is also shown. Note that Y axis limits are different for each subplot. Bottom row: same for the ocean heat content anomalies (with respect to the 1950-2003 mean, $[1 \times 10^{22} J]$), for years 1960, 1980, and 2000. The emulator performance, of course, will be different for other times not shown here.

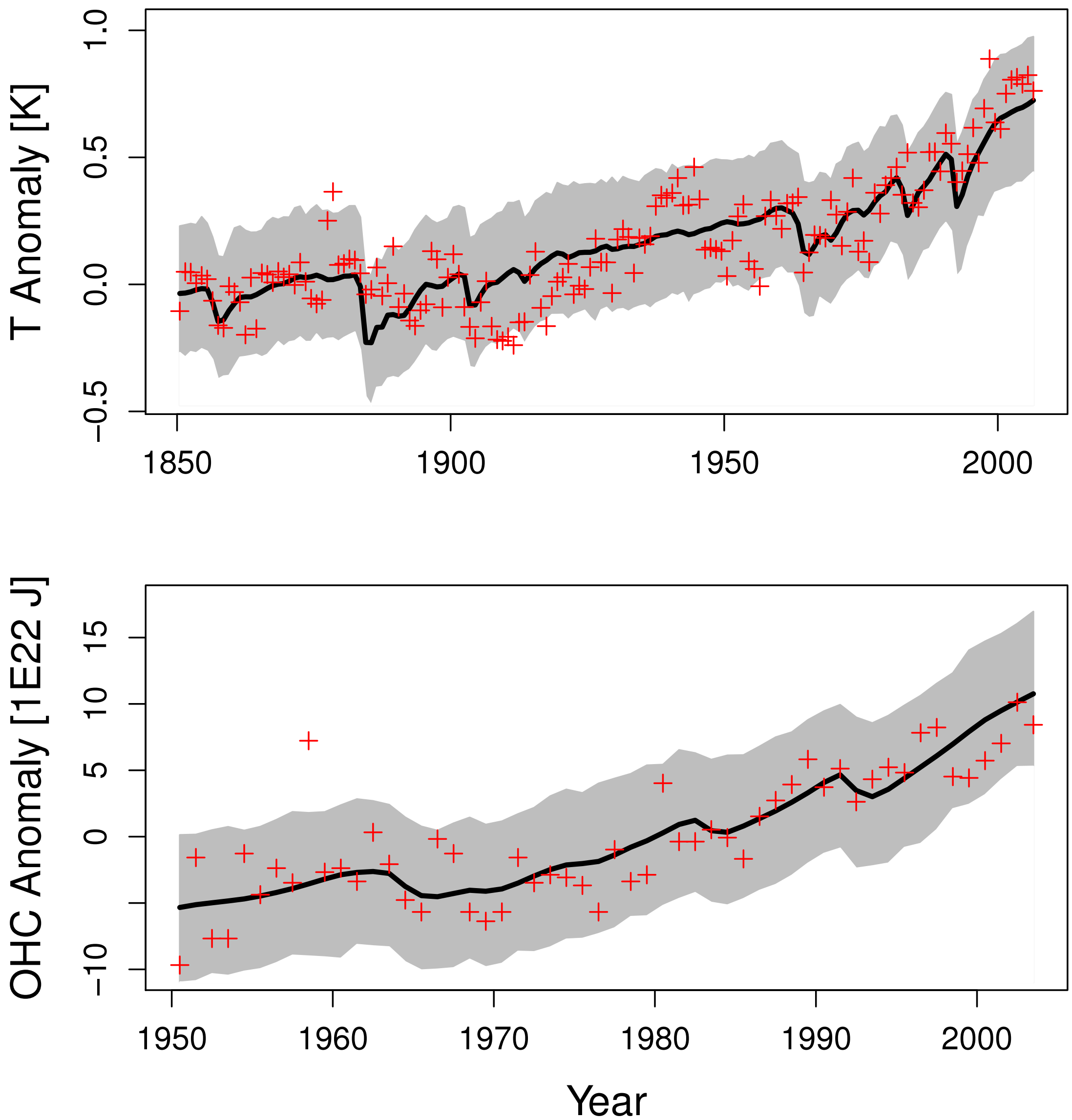

Figure 2: Probabilistic model hindcasts (grey shaded area), maximum posterior probability model output ('best fit', black line), and corresponding observations (red crosses) for the NON-UNIF assimilation experiment: (a) global average atmospheric surface temperature anomaly with respect to 1850-1899 mean [K] with corresponding observations of above surface / ocean surface temperatures from the HadCRUT3 dataset [*Brohan et al.*, 2006]; (b) upper ocean (0-700m) heat content anomaly with respect to 1950-2003 mean [1E22J], and observations from *Domingues et al.* [2008]. The grey area denotes the 95% credible intervals for model output taken from a 1000-member subsampled MCMC chain, with corresponding AR1 error processes (and bias terms for temperature) added. For the AR1 process simulations, the σ and ρ parameters were taken from the corresponding chain member. For the best fit model output for temperature, the maximum posterior probability model output was combined with the corresponding bias term.

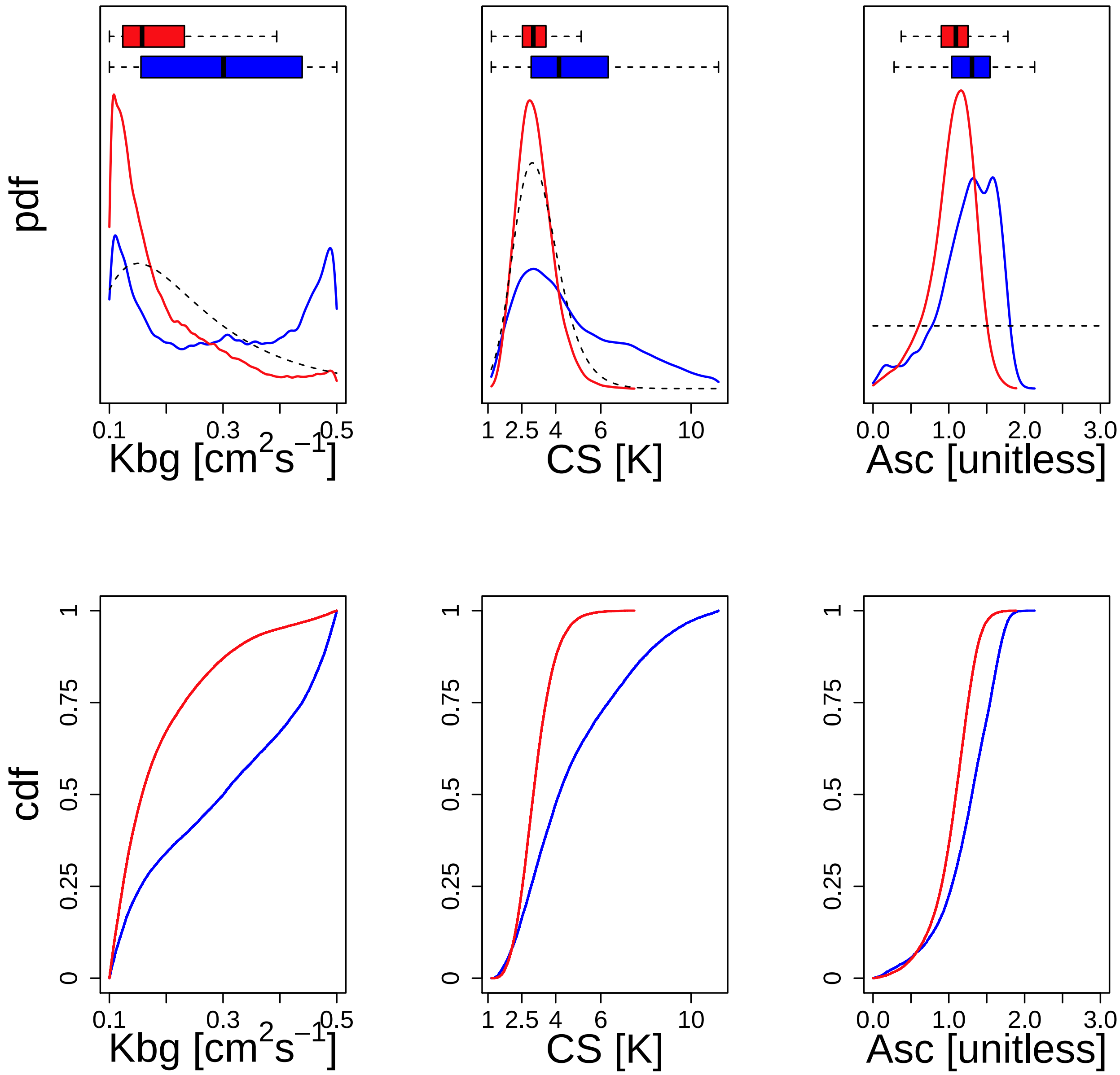

Figure 3: Posterior pdfs (top row) and cdfs (bottom row) for model parameters obtained using both temperature and ocean heat content observations. Red: for the NON-UNIF experiment; blue: for the UNIF experiment. The dashed probability distribution lines represent the priors used in the NON-UNIF experiment. The dashed whiskers in the box-and-whisker plots extend to the most extreme data point which is no more than 1.5 interquartile ranges from the box.

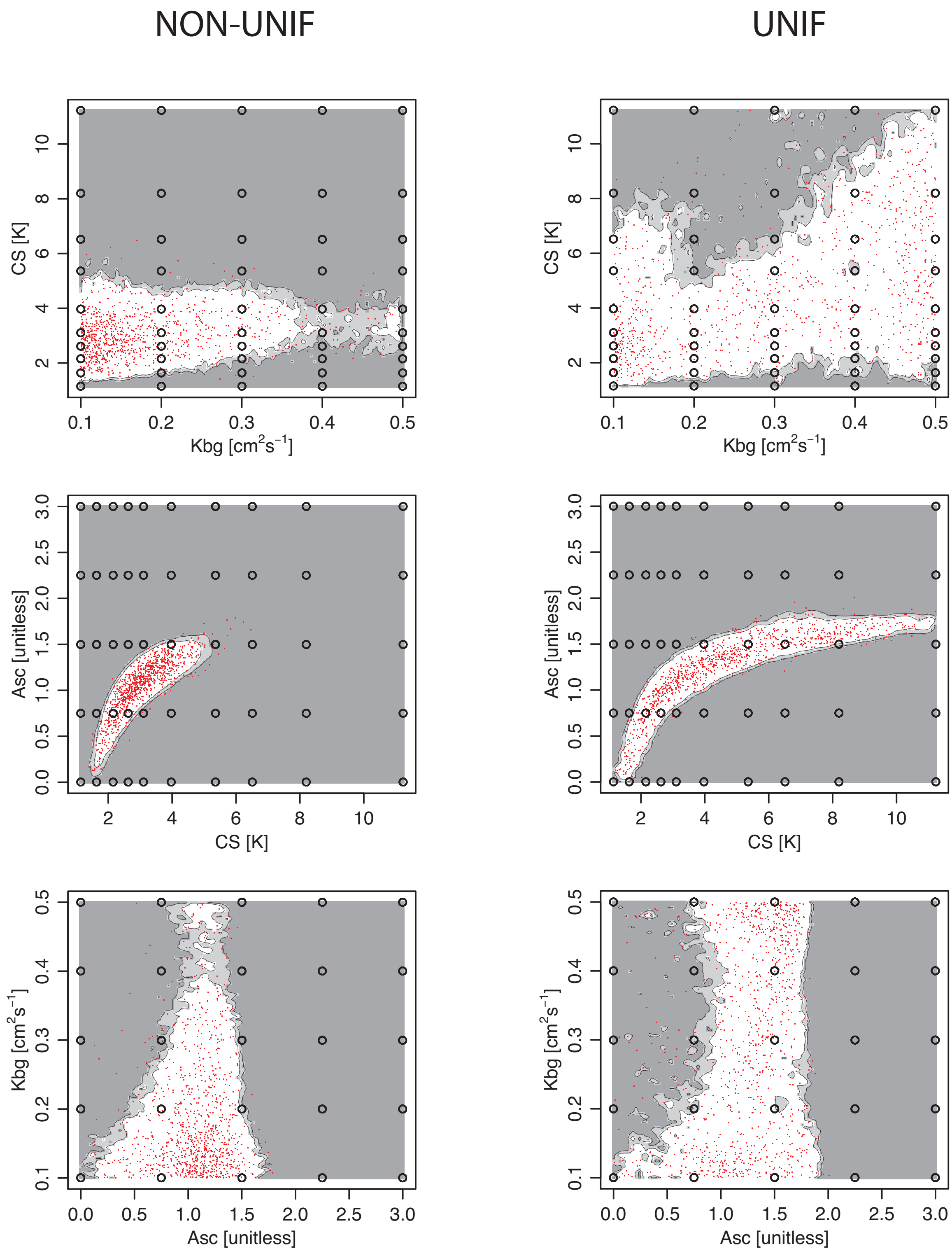

Figure 4: Bivariate joint pdfs for model parameters. Left: for the NON-UNIF experiment, right: for the UNIF experiment. The contour lines delineate the 90% and 95% posterior credible intervals. A 1000-member thinned MCMC chain is plotted using red dots. Parameters used for the UVic ESCM ensemble are shown in thick black circles.